ACS APPLIED MATERIALS & INTERFACES

Research Article

www.acsami.org

Fabrication of Inkjet-Printed Gold Nanostar Patterns with Photothermal Properties on Paper Substrate

Mykola Borzenkov,*[,†] Anni Määttänen,*[,‡] Petri Ihalainen,[‡] Maddalena Collini,[†] Elisa Cabrini,[§] Giacomo Dacarro,[§] Piersandro Pallavicini,[§] and Giuseppe Chirico[†]

[†]Department of Physics "G. Occhialini", Nanomedicine Center, University of Milano-Bicocca, piazza della Scienza 3, 20126 Milan, Italy

[‡]Laboratory of Physical Chemistry, Center for Functional Materials, Åbo Akademi University, Porthaninkatu 3-5, 20500 Turku, Finland

[§]Department of Chemistry, University of Pavia, viale Taramelli 12, 27100 Pavia, Italy

Supporting Information

ABSTRACT: Inkjet printing technology has brought significant advances in patterning various functional materials that can meet important challenges in personalized medical treatments. Indeed, patterning of photothermal active anisotropic gold nanoparticles is particularly promising for the development of low-cost tools for localized photothermal therapy. In the present work, stable inks containing PEGylated gold nanostars (GNSs) were prepared and inkjet printed on a pigment-coated paper substrate. A significant photothermal effect ($\Delta T \cong 20$ °C) of the printed patterns was observed under near infrared (NIR) excitation of the localized surface plasmon resonance (LSPR) of the GNS with low laser intensity ($I \cong 0.2$ W/cm^2). Besides the pronounced photothermal effect, we also demonstrated, as an additional valuable effect, the release of a model fluorescent thiol-terminated Bodipy dye (BDP-SH) from the printed gold surface, both under bulk heating and NIR irradiation. These preliminary results suggest the way of the development of a new class of low-cost, disposable, and smart devices for localized thermal treatments combined with temperature-triggered drug release.

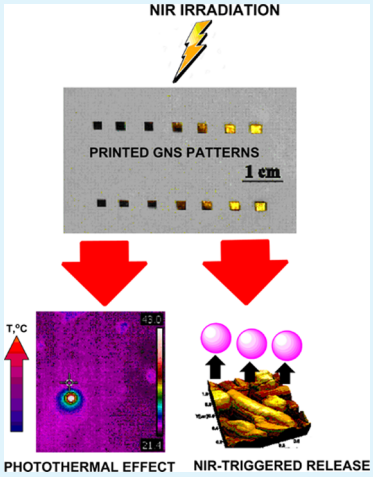

KEYWORDS: *gold nanostars, inkjet printing, NIR irradiation, photothermal effect, controlled release*

INTRODUCTION

Inkjet printing technology is becoming an attractive patterning technique among other methods (e.g., vapor deposition, photolithography, etc.) mainly due to easy and high speed one-step processing, low working temperatures, reduced amount of toxic wastes, and reduced costs.[1,2] Inkjet printing has been successfully applied to pattern various functional materials such as transistors, integrated circuits, conductive polymers, ceramics, etc.[3,4] In addition, recently inkjet printing has been also successfully adapted to print a wide range of materials (including also biomaterials) for applications in biology and medicine.[5−11] The formulation of suitable inks for deposition of functional materials is considered to be a major factor in successful application of inkjet printing technologies.[12] Inks made of metal nanoparticles have significant advantages over other formulations, and they are widely used for their relevant conductive and thermal properties.[1,13] Within the range of existing metal nanoparticles, gold nanoparticles are most commonly used for nanomedical applications[14−16] since gold is chemically inert, displays excellent resistance to oxidants and acids, has high conductivity when thermally sintered,[17] is not cytotoxic, and has a high affinity for thiol-containing biomolecules. Relevantly to this paper, anisotropic (i.e., nonspherical) gold nanoparticles feature large near infrared absorptions in the biotransparent range (~750−1100 nm) due to their localized surface plasmon resonances (LSPRs). These LSPRs, once excited, thermally relax, producing highly localized and adjustable thermal loads that can be used for hyperthermal treatments.[18−21] In addition, local photoinduced hyperthermia could also be applied to the localized laser-triggered release of surface-bound or encapsulated drugs for local pharmacological therapies.[22] In this context it must also be stressed that printing of spherical gold nanoparticles onto various substrates (including paper) has been recently applied to assemble analytical and diagnostic tools.[9,23−28] The combination of the benefits of inkjet printing technologies with the photothermal properties of anisotropic gold nanoparticles can produce novel biomedical devices. However, the investigation of photothermal properties of such

Received: March 10, 2016
Accepted: March 31, 2016
Published: March 31, 2016

DOI: 10.1021/acsami.6b02983
ACS Appl. Mater. Interfaces 2016, 8, 9909−9916

nanoparticles printed onto flexible substrates for fabrication of medical devices has not been described.

In this study we use a well-characterized subcategory of anisotropic gold nanoparticles, namely, gold nanostars (GNSs). Such a name is due to their resemblance with the pictorial representation of stars, as they feature a core with 4−6 branches protruding from it. GNSs are prepared with seed-growth syntheses using weakly interacting surfactants such as lauryl sulphobetaine (LSB)[29] and feature one main intense LSPR extinction band in the NIR range (750−1100 nm), whose wavelength maximum can be sharply regulated by synthetic conditions. Moreover, they feature a much weaker LSPR band at 500−550 nm, responsible for the huge surface-enhanced Raman signal (SERS).[29,30] In addition, when laser-irradiated at the wavelength of their NIR LSPR band GNSs exhibit excellent transduction of absorbed light into heat.[31] GNSs have specific absorption rates (SARs) as high as 80 kW/g, displaying a local increase in temperature as high as 12 °C at a 10 nm distance from the gold nanostar surface in aqueous solution, making them more efficient than gold nanorods and magnetite nanoparticles in inducing localized temperature jumps.[18] Such temperature jumps are dramatically larger when GNSs are prepared as monolayers on dry bulk surfaces.[21,32] Finally, the charge and hydrophobicity of the GNSs coating can be finely tuned thanks to their ability to bind a wide range of molecules with high surface density, thus enhancing the possibility to use them as nanosensors and/or drug delivery platforms.[33,34] By choosing the proper molecular coating, e.g., a thiol-functionalized poly(ethylene glycol) (PEG-SH), an outstanding solubility and stability in a variety of solvents and media is imparted to the GNS.[29,35]

Due to this broad spectrum of potentially useful properties, GNSs prepared in the presence of LSB and coated with PEG-SH (average molecular weight 5000 g/mol) were selected in this paper for ink preparation, under synthetic conditions leading to their main LSPR centered at ∼760 nm.[29] This work has been carried out in the perspective of GNS inkjet printing for the manufacturing of flexible substrates with photothermal activity for localized and personalized photothermal medical treatments. In order to demonstrate this possibility, pigment-coated paper was chosen as a printing substrate. Paper is a sustainable and recyclable material, and its physicochemical properties (topography, roughness, stiffness, surface energy, polarity, porosity, and pore geometry) can be modified conveniently by various coating materials, methods, and surface treatments depending on the requirements of the targeted applications.[36] Therefore, for example, recently inkjet printed plasmonic silver- or gold-based inks on paper have emerged as a potential low-cost replacement for conventional nanofabricated SERS devices.[28,36,37] Inkjet printing with inks of different GNS concentrations on pigment-coated paper substrate was carried out with variation of drop density (δ, drops/mm^2) and of layer counts. The photothermal response of the resulting patterns was studied under NIR irradiation. In addition, the model organic compound, the fluorescent Bodipy-thiol (BDP-SH) dye, was bound to the gold surface, and its photothermally induced release from the printed patterns was demonstrated.

EXPERIMENTAL DETAILS

Chemicals and GNS Synthesis. All chemicals were purchased from Sigma-Aldrich and used as received. BDP-SH was synthesized as reported previously.[38] GNS solutions were obtained by a seed growth synthesis with the zwitterionic surfactant, lauryl sulfobetaine (LSB), as already described.[29] After the growth process, GNS solutions were ultracentrifuged, the supernatant discarded, and the GNS pellet redissolved in the starting volume of bidistilled water, and the GNSs were coated with PEG thiols (see description below). The detailed information about chemicals and GNS synthesis is provided in the Supporting Information (S1 *Chemicals and GNS preparation*). Previous characterization studies showed that these have average branch length of ∼30 nm with negative zeta potential, ζ-potential = −15 mV, in pure water.[29]

Coating of GNS with PEG-SH. GNSs were coated by simultaneously adding 200 μL of a 10^{-3} M aqueous solution of PEG-SH (average molecular weight 5000 g/mol) to 10 mL of a GNS solution prepared as described above. The obtained solution was allowed to equilibrate for 3 h at room temperature while gently shaken on a reciprocating shaker. Excess of PEG-SH was removed by ultracentrifugation (25 min, 13000 rpm), supernatant discarding, and pellet redissolution in 10 mL of bidistilled water. The cleaning cycle was repeated two more times to ensure thorough elimination of unbound PEG-SH and LSB. The latter is almost completely displaced also from the GNS surface after such treatment.[29] The concentration of the resulting PEGylated GNS solutions is 0.060 mg Au/L, determined by ICP-OES as described previously.[29] More concentrated GNS solutions were prepared using larger GNS volumes in the PEGylation step (100 mL instead of 10 mL), and redissolving the GNS pellet after the last ultracentrifugation cycle in 10 or 1 mL of bidistilled water, obtaining 10-fold (0.6 mg Au/mL) and 100-fold (6 mg Au/mL) concentrated solutions, respectively.

Formulation of the GNS Inks. The inks were formulated by adding 1,2-ethanediol (20% vol.) and 2-propanol (10% vol.) to the aqueous PEGylated GNS solution (70% vol.) to adjust the viscosity and surface tension to suitable values for inkjet printing (1.92 cP and 40 mN/m, respectively).[39] The final concentrations of GNS (C_{GNS}) in the prepared inks were thus 0.042, 0.42, and 4.2 mg/mL.

Paper Substrate. A proprietary multilayer pigment-coated paper was used as the print substrate.[40,41] This paper substrate was specially designed for printed electronics and contains a barrier layer underneath a thin porous top coating layer consisting mainly of precipitated calcium carbonate (PCC) pigments and a latex binder. The top coating enhances the print resolution and adhesion as well as reduces ink smearing. Moreover, the barrier layer prevents the functional inks from penetrating too deep inside the paper structure. This substrate was fabricated using commonly used coating components in the papermaking industry. Therefore, the substrate is recyclable like any other ordinary coated paper used in the graphical printing industry. More detailed information about the substrate, its fabrication, and physicochemical properties is given elsewhere.[41,42]

Inkjet Printing of GNS Inks. Inkjet printing was performed with Dimatix Materials Printer (DMP-2800, FUJIFILM Dimatix, Inc., Santa Clara, USA). The printing process was performed in ambient conditions using a single nozzle with a nominal droplet volume of 10 pL, 16 ± 3 V firing voltage, 2 kHz firing frequency, and a custom waveform to ensure optimal droplet formation (see movie in Supporting Information "Formation of drops"). Various drop density values ($1178 \leq \delta \leq 40401$ drops/mm^2) and layer counts (1−7) were used to print the GNS patterns (areas, A: 1 mm^2, 4 mm^2, 9 mm^2, and 16 mm^2). Additional details about the printing process are provided in Supporting Information (see S2 Inkjet printing of GNS inks).

Atomic Force Microscopy. An NTEGRA PRIMA (NT-MDT, Russia) atomic force microscope (AFM) was used for topographical analysis and thickness determination of the inkjet-printed GNS films. The images (1024 pixels × 1024 pixels) were captured in intermittent-contact mode in ambient conditions using silicon cantilevers with a nominal tip radius of 10 nm (model: NSG 10, NT-MDT, Russia). The scanning rate and damping ratio were 0.2−0.30 Hz and 0.6−0.7, respectively. Image analysis was done using SPIP image analysis software (Image Metrology, Denmark).

Near Infrared Irradiation of Printed GNS Patterns. The patterns were irradiated at λ = 800 nm (Tsunami, Spectra Physics, CA, pulse repetition rate 80 MHz, pulse width 200 fs). The substrate temperature changes were monitored by means of a Thermovision

DOI: 10.1021/acsami.6b02983
ACS Appl. Mater. Interfaces 2016, 8, 9909−9916

camera (FLIR, E40, USA) with supporting software. The temperature was monitored in time on a Region of Interest (ROI) comprising the irradiated area. The maximum temperature within the ROI was taken as the measure of the temperature increase on the pattern induced by the NIR irradiation, and it was followed in time until the steady state was reached. All the temperature increase data refer to the difference between this steady-state value, measured under continuous irradiation, and room temperature.

Conjugation of BDP-SH onto Printed GNS Patterns. Before exposure to BDP-SH solutions, the patterns were rinsed with ethanol and dried with nitrogen gas. The patterns were first exposed to 200 μL of BDP-SH aqueous solution, prepared by diluting the stock dye solution (C_{dye} = 0.01 M in ethanol) with Milli-Q water at the final dye concentration of 16 μM, for 24 h at room temperature in the dark. Then the solution was removed from the patterns, and the patterns were washed immediately with ethanol (5 times) to remove the excess of dye and dried with nitrogen gas. Ethanol was used as washing medium since the hydrophobic BDP dye is more soluble in ethanol than in water.

Spectroscopy Measurements. The emission spectra of BDP-SH were recorded using an Eclipse spectrofluorimeter (Varian, AU). The detector gain (800 V) and the slits size (exc. slit 5 nm; em. slit 10 nm) were kept constant over all the measurements. BDP-SH was excited at 525 nm, and its maximum emission intensity was observed at 539−541 nm. The temperature control was obtained with a Cary Temperature Controller connected to the Varian spectrofluorimeter. Absorbance spectra of dye, bare, and PEGylated GNS aqueous solutions were recorded using an UV/vis/NIR spectrophotometer V-570 (Jasco, J).

RESULTS AND DISCUSSION

Properties of Bare and PEGylated GNSs. The GNSs employed in this study were prepared using the weak LSB surfactant as the directing agent. They are prevalently pentatwinned branched nanoparticles as shown in Figure 1A

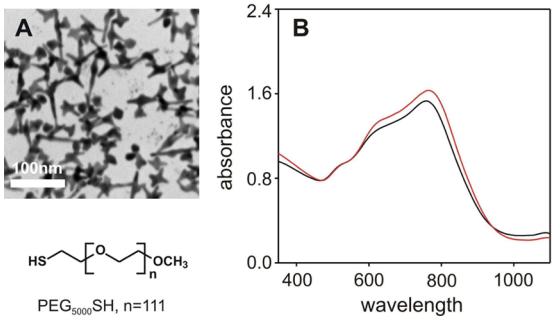

Figure 1. Structural and spectroscopic characterization of GNS. Panel A: exemplary TEM image of PEGylated GNSs and chemical structure of employed PEG. Panel B: extinction spectra of bare (black line) and PEGylated GNSs (red line) showing the red shift of LSPR.

with a minor component in the product consisting in monocrystalline regular 4-branched GNSs.[29,35] The extinction spectrum shows also a minor component at 520 nm, arising from the spherically symmetric plasmon resonance on the nanoparticle core and two NIR components at about 630 nm (shoulder) and 760 nm (main peak) as shown in Figure 1B. The NIR extinction bands are due to the resonant electron oscillations along the branches.[29]

Preliminary spectroscopic analysis of bare (uncoated) GNSs in the ink medium indicated instability and tendency to aggregate, as typical for uncoated gold nanoparticle solutions when solvents different from water are added. This could lead to nozzle clogging during inkjet printing, and such formulations were discarded. In order to increase the stability and prevent aggregation, GNSs were coated with PEG thiols (see formula in Figure 1). PEG thiols are frequently used as coatings for gold nanoparticles to increase the stability, dispersibility, and biocompatibility of the particles for both in vitro[43,44] and in vivo applications.[45] GNSs coated with PEG-SH become soluble in a variety of solvents, from water to hydrophobic ones,[29] due to the amphiphilic nature of the poly(ethylene glycol) chains. PEG-SH coating causes LSPR of GNSs to red-shift ∼10 nm, due to the slight local increase in the refractive index related to thiols grafting on the gold surface.[29] GNSs coated with PEG-SH are stable even after repeated ultracentrifugation cycles and show long time stability in the water/2-propanol/1,2-ethanediol media used to prepare inks. No spectral changes or precipitation were observed over time (more than 3 weeks), indicating good stability of these formulations.

AFM Topographical Characterization of the Inkjet-Printed GNS Patterns. The GNSs were inkjet printed on the PCC-coated paper using inks with increasing GNS concentrations, from 0.042 to 4.2 mg/mL. The PCC-coated paper (Figure 2), employed here as the printing substrate, offers suitable nanoporosity (∼average pore diameter 90 nm, top coating thickness <10 μm) to allow partial penetration of the ink into the top coating matrix. This feature increases the adhesion and prevents the GNS to be totally immersed deep into the base paper.[42] The coverage of the paper varied with the concentration of GNS in the inks, with the drop density (δ) and with the number of printed layers. A fully covering GNS film was not achieved by a single printed layer, even when using the highest print density (δ = 40401 drops/mm^2) and the highest tested GNS concentration in the ink. The AFM topography of the paper substrate after printing of a single GNS layer (C_{GNS} = 4.2 mg/mL, δ = 40401 drops/mm^2) shows only randomly oriented rod-shaped PCC pigments with size of 0.5−1.5 μm with no clear indication of surface-bound GNS layer (Figure 2b), and this is very similar to the AFM topography of the bare paper (Figure 2a). This indicates that most of the GNSs have penetrated inside the PCC matrix. However, due to the coffee stain phenomenon there is a thicker layer of GNS accumulated at the edge of the pattern. This is clearly seen in the optical image as a golden color at the edge compared to the dark middle area (see Supporting Information, Figure S1). The thicker area is also observed in the middle of the AFM image as a more blurred area, where the PCC pigments are not so clearly visible due to the presence of a higher amount of GNS near the surface (see Supporting Information, Figure S1). Clearly observable surface films of GNS were only obtained when multiple layers were inkjet printed on the same area. Figure 2c shows an example of a fully covering GNS film (obtained by printing 6 layers with δ = 40401 drops/mm^2 and GNS concentration of 0.42 mg/mL) where the details of the PCC matrix are no longer visible.

SEM images of printed GNS patterns (see Supporting Information, S4) follow the trend observed in AFM images (for example PCC pigments are still clearly seen for patterns printed with a single print layer with δ = 40401 drops/mm^2 and C_{GNS} of 4.2 mg/mL).

NIR Irradiation of Printed GNS Patterns. The laser-induced photothermal response of printed GNS patterns (dry, exposed to air at room temperature) was obtained by irradiating with a NIR laser tuned at λ = 800 nm, i.e., near to the NIR LSPR (absorption maximum is 770 nm) of the PEG-SH-coated GNS. A steep temperature increase turning into a plateau after 15 s was observed in all cases[21] (see Supporting

DOI: 10.1021/acsami.6b02983
ACS Appl. Mater. Interfaces 2016, 8, 9909−9916

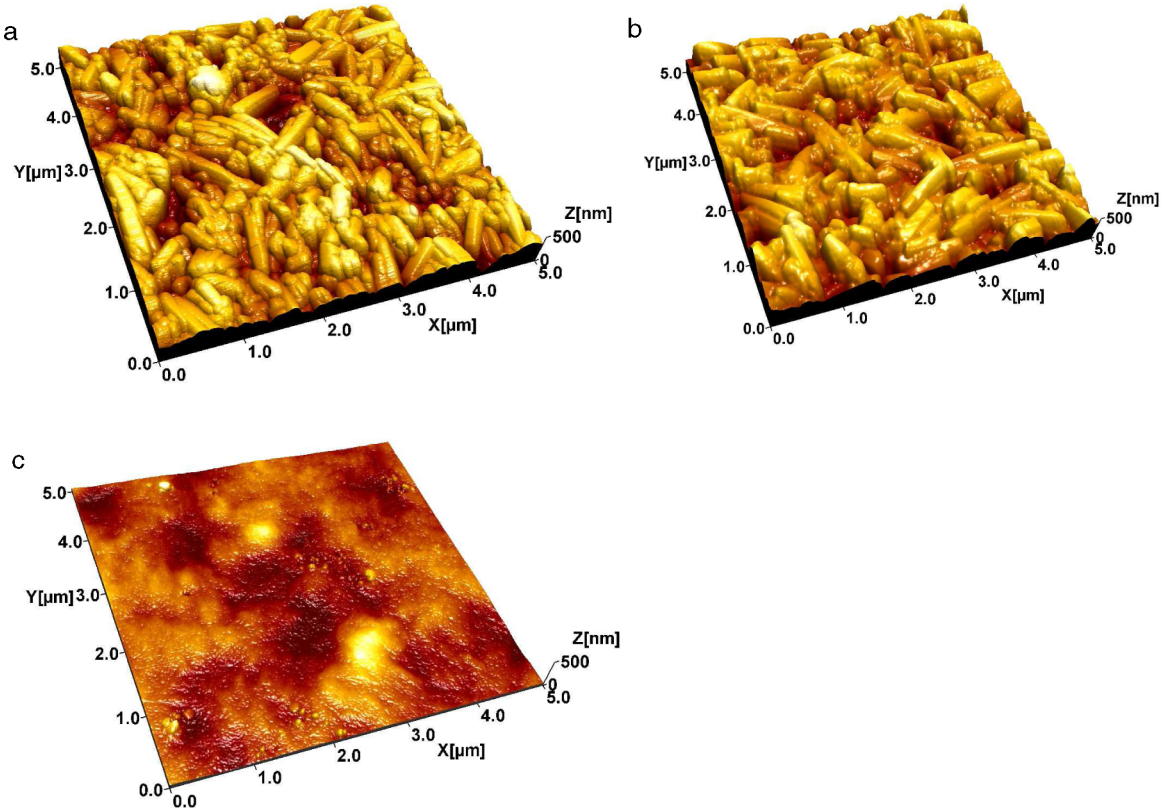

Figure 2. (a) Small-scale AFM topographical image of the paper substrate showing the rod-like PCC pigment particles. (b) Small-scale AFM topographical image showing that the PCC pigment particles are still clearly visible after printing a single layer with δ = 40401 drops/mm^2 and C_{GNS} of 4.2 mg/mL. (c) Small-scale AFM topographical image of the surface-bound GNS film obtained by printing 6 layers with δ = 40401 drops/mm^2 and C_{GNS} = 0.42 mg/mL.

Information, S5). The observed temperature jump, ΔT_{max}, is the difference between the plateau temperature and the starting (room) temperature. Figure 3 shows how ΔT_{max} of the printed patterns increases with the laser power, and these results are in agreement with previous observations.[18,21,46] In fact, we have previously reported that aqueous solutions of GNSs, when irradiated at λ = 800 nm and at an irradiance I_{exc} = 14 W/cm^2, undergo an increase in temperature with $\Delta T_{max} \approx$ 30 °C.[18] What is observed here is also very similar to what we have already described when irradiating dry GNS monolayers on a glass surface.[32] However, as it clearly seen in Figure 3, we are able to reach a significantly higher temperature jump on the printed GNS patterns even at much lower laser intensities (I_{exc} < 0.8 W/cm^2), due to the absence of the thermal dissipation from the bulk solvent (water) that has a high thermal capacity. As a comparison, control experiments performed by irradiating the blank paper substrate at the same laser intensities showed an almost negligible photothermal response ($\Delta T \leq$ 0.4 °C). A measurable thermal load (ΔT_{max} > 20 °C) was obtained even from the GNS patterns printed with the lowest concentration ink. Indeed, the photothermal effect (ΔT_{max}) is a function of both laser intensity and the ink concentration. The dependence on the laser intensity is well described by a linear trend up to $I_{exc} \approx$ 0.6 W/cm^2, and then a saturation effect appears suggesting the balancing effect of two mechanisms. At low irradiation intensity, we can assume that the temperature increase ΔT_{max} is given by eq 1

$$\Delta T_{max} \sim \Delta I \simeq I_{exc}(1 - e^{C\varepsilon\Delta x}) = \beta I_{exc} \quad (1)$$

where ΔI is the loss in excitation intensity due to nanoparticle absorption, written here as the difference between the excitation and the transmitted beam; C is the GNS concentration in inks; Δx is the layer thickness; and ε is related to the absorption cross section of GNS. Equation 1, however, would predict a linear behavior as a function of I_{exc} for all the intensity range. A second mechanism that can drain heat

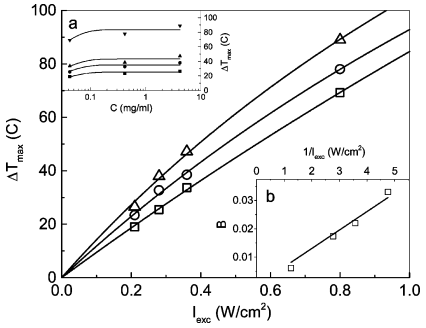

Figure 3. Dependence of temperature increase of GNS pattern printed on PCC paper substrates with inks at different nanoparticle concentration as a function of the NIR laser intensity: C_{GNS} = 0.042 mg/mL, 121203 drops/mm^2 (open squares); C_{GNS} = 0.42 mg/mL, 121203 drops/mm^2 (open circles); C_{GNS} = 4.2 mg/mL, 40401 drops/mm^2 (open triangles). The lines are the best linear fit to the data with eq 3. Insets: (a) reports the same data as a function of the concentration globally fit to eq 4b. (b) Shows the behavior of the best fit parameter B, which is linear in $(I_{exc})^{-1}$, as expected. The error bars are within the point size. The best fit parameters are discussed in the text.

DOI: 10.1021/acsami.6b02983
ACS Appl. Mater. Interfaces 2016, 8, 9909−9916

from the irradiated GNS layer is due to the exchange with the surrounding environment. The experimental maximum temperature increase would then be given by an implicit eq 2 that, at the first order, can be stated as

$$\Delta T_{max}^{exp} \simeq \Delta T_{max} - \kappa_{eff}(T)\Delta T_{max}^{exp} \quad (2)$$

where $\kappa_{eff}(T)$ is an effective adimensional parameter, related to the thermal conductivity of the environment divided by the mass and the specific heat of the GNS, for unit time and area. Its temperature dependence, primarily due to the air thermal conductivity, can be obtained by a series expansion as a function of the temperature increase, $\kappa_{eff}(T) = \kappa_{eff}^0 + \frac{\partial \kappa_{eff}(T)}{\partial T}\Delta T + o(\Delta T^2)$, that inserted in eq 2 leads to eq 3

$$\Delta T_{max}^{exp} \simeq \frac{\Delta T_{max}}{1 + \kappa_{eff}^0 + \frac{\partial \kappa_{eff}}{\partial T}\Delta T_{max}} = \frac{\beta I_{exc}}{1 + \kappa_{eff}^0 + \frac{\partial \kappa_{eff}}{\partial T}\beta I_{exc}} = \frac{K I_{exc}}{1 + I_{exc}/I_{sat}} \quad (3)$$

The solid lines in Figure 3 are the best fits of eq 3 to the data collected as a function of I_{exc}. It has to be noted that at low intensities, $\Delta T_{max}^{exp} \approx K I_{exc} = \frac{\beta}{(1+\kappa_{eff}^0)} I_{exc}$. The slightly different initial slopes of the data in Figure 3 indicate that the linear coefficient K does not have a marked dependence on the GNS concentration, even when it spans 2 orders of magnitude (0.042 mg/mL $\leq C \leq$ 4.2 mg/mL). By combining eq 1 and eq 3, we can describe also the dependence of ΔT_{max}^{exp} upon the concentration C

$$\Delta T_{max}^{exp} = \frac{I_{exc}(1 - e^{-C\varepsilon\Delta x})}{1 + \kappa_{eff}^0 + \frac{\partial \kappa_{eff}}{\partial T} I_{exc}(1 - e^{-C\varepsilon\Delta x})} = \frac{(1 - e^{-C\varepsilon\Delta x})}{\frac{1+\kappa_{eff}^0}{I_{exc}} + \frac{\partial \kappa_{eff}}{\partial T}(1 - e^{-C\varepsilon\Delta x})} \quad (4a)$$

The maximum temperature increase (inset in Figure 3a) at different excitation intensities is globally fitted to eq 4a as a function of the concentration by means of the trial function

$$\Delta T_{max} = \frac{1 - e^{-AC}}{B + D(1 - e^{-AC})} \quad (4b)$$

A and D can be determined as shared parameters, and $B = \frac{1+\kappa_{eff}^0}{I_{exc}}$ is determined for each set of intensity data. In particular, as shown in Figure 3b (inset), the B parameter scales inversely with the excitation intensity as expected. The value of A (30 ± 11. l/g) is consistent with an absorption cross section in the range $\approx 10^{-10}$ cm^2 < σ < 10^{-9} cm^2 when an average thickness value is assumed to be about 1 μm. This value is consistent with the highest value ($\cong 4 \times 10^{-10}$ cm^2) computed with the Discrete Dipole Approximation method for nonspherically symmetric gold nanoparticles.[47] The term D, related to the temperature dependence of the air thermal conductivity, is positive as expected.[48] However, this parameter is poorly determined from the fit to eq 4b since it multiplies the absorption term $1 - e^{-AC}$, which is non-negligible only for the lowest ink concentration C = 0.042 mg/mL.

Marked nonlinear responses appear also when studying the impact of increasing of drops density values on the photothermal effect of printed GNS. We have investigated in detail the patterns printed with inks at the lowest and the highest concentration of GNS with different amounts of printed drops/mm^2, and the results are reported in Figure 4.

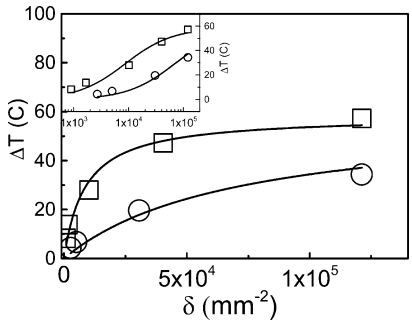

Figure 4. Increase of the temperature measured on the patterns under NIR irradiation as a function of the drops density δ (drops/mm^2) used to print GNS patterns. The GNS ink concentrations were: C_{GNS} = 0.042 mg/mL (circles) and C_{GNS} = 4.2 mg/mL (squares); laser intensity 0.36 W/cm^2. The solid lines are the best fit of eq 4 to the data. In the inset, the same data are plotted in a logarithmic scale in order to show the low drop density region in a clearer way. The error bars are within the point size.

The thermal response increases also with the drop density, δ (i.e., when decreasing the drop spacing). The nonlinearity appears already for $\delta \approx$ 10000 drops/mm^2 (for C_{GNS} = 4.2 mg/mL) and for $\delta \approx$ 25000 drops/mm^2 (for C_{GNS} = 0.042 mg/mL). It is noteworthy that also these sets of data can be fit to eq 4b in which the fitting parameter is an effective concentration related to the drop density δ.

Since a substantial photothermal effect is observed under NIR irradiation even for patterns that do not correspond to full coverage of the paper with GNS (as seen in Figure 2b), it can be concluded that the presence of the full GNS film is not necessary to have a significant local temperature increase on NIR irradiation. Nevertheless, the presence of full coverage could be important to allow a more abundant grafting of molecules on the printed patterns, capable to subsequently undergo a switchable release triggered by irradiation, as illustrated below.

Release of BDP-SH Dye Bound to the Printed Gold Surface under NIR Irradiation. Besides the direct thermal effect of printed GNS patterns under NIR irradiation, we studied also the possibility to thermally induce the release of molecules from the printed gold surface triggered by the NIR irradiation. For this purpose the fluorescent Bodipy dye with terminated thiol group was chosen as a model compound.[38] This choice is justified by the good stability of Bodipy dyes in aqueous solutions and by their high fluorescence quantum yields.[46] The chemical structure of the dye is shown in Scheme 1.

In a previous work, we demonstrated that the release of BDP from the surface of GNS cocoated with PEG-SH and BDP-SH is induced in an aqueous solution either by bulk heating or NIR irradiation.[46] In the present study BDP-SH was conjugated to the printed gold pattern via a thiol-exchanging process that occurred by dipping the printed GNS patterns in an aqueous solution containing excess BDP-SH dye and promoted by the less hydrophilic character of BDP-SH with respect to PEG-SH.[38,49] It has to be noted that such an approach is possible due to the resistance of PCC-coated paper to water imbibition.

DOI: 10.1021/acsami.6b02983
ACS Appl. Mater. Interfaces 2016, 8, 9909−9916

Scheme 1. Chemical Structure of BDP-SH Dye

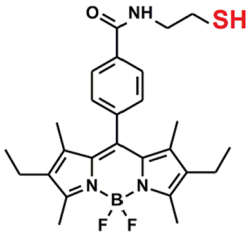

The amount of bound dye was estimated from the difference of absorbance between BDP-SH solutions (200 μL) before dipping and after removing the paper sheet (4 mm^2) featuring the gold patterns. The absorbance spectra were measured 5 times in each case. The GNS patterns printed on PCC substrates with ink concentration C_{GNS} = 0.42 mg/mL (δ = 20402 drops/mm^2) and C_{GNS} = 4.2 mg/mL (δ = 20402 drops/mm^2) were employed for this experiment. The amount of dye bound onto the printed gold surface was 760 (±2) pmol and 1020 (±2) pmol, for the two substrates, respectively. These values correspond to approximately 0.38 μg and 0.51 μg of dye bound on the two samples, respectively. The surface density, referred to the printed paper area (4 mm^2), is 1.14 × 10^{16} and 1.53 × 10^{16} molecules/cm^2, with a dramatic increase of 2 orders of magnitude with respect to the 1.2 × 10^{14} molecules of BDP-SH that were found to be grafted on a monolayer of spherical silver nanoparticles adhering to a flat glass surface.[38] Such an increase is particularly interesting in the perspective of loading and releasing considerable drugs quantities. It is due to the multilayered nature of the printed GNS patterns, indicating that also the underlying GNS can be reached by the soaking solution and be loaded by a molecule equipped with a proper grafting group.

First, the dye release from the printed GNS surface was induced by bulk heating. The patterns were put in cells and covered with 100 μL of water (approximately 2 mm of water depth). The samples were then heated in a thermostat at 42 and 60 °C. The paper sheets with the printed patterns were removed, and the emission spectra of the water solution were collected at 20 °C, allowing us to detect the amount of the dye released as supernatant according to the calibration curves reported in the Supporting Information (see sections S6 and S7). The amount of released BDP dye from GNS was found to be proportional to the heating temperature and duration, as found previously for bulk GNS solutions.[46] As an example, exposure at 42 °C for 40 min led to the release of 13.6 ± 1% of the grafted BDP-SH from patterns printed at 20402 drops/mm^2 with C_{GNS} = 0.42 mg/mL.

The spontaneous release of weakly bound dye can be excluded by the following control experiment. Printed GNS patterns with bound dye and covered with water were stored under ambient conditions. Emission spectra were recorded at regular intervals, indicating less than 2% of dye release during long observation time (4 days). This confirms that washing with ethanol removed the BDP-SH molecules possibly adhering to the printed surface by nonspecific hydrophobic interactions instead of Au−S bond formation.

Nonspecific adsorption of dye to the bare paper surface could also impact the evaluation of the dye release. Therefore, samples of bare PCC paper (4 mm^2) were incubated overnight in BDP solutions with the same concentration of dye, then washed with ethanol 5−6 times, and dried (~100 pmol of adsorbed dye before the washing step). Some BDP dye molecules can still be found inside the porous paper structure even after this repeated washing procedure, as was confirmed by fluorescence microscopy imaging. However, when the samples were put back into the incubation wells, covered with 100 μL of water and heated for 15 min at 42 °C, very low values of released dye (≤1.2% in comparison with values of released dye from printed gold surfaces) were observed in the supernatant. This leads to the conclusion that even nonspecific adsorption of dye took place, and no thermally triggered release of BDP molecules occurred in the case of bare paper.

Fluorescence microscopy images of GNS patterns (C = 0.42 mg/mL, δ = 30603 drops/mm^2) taken before and after the dye release experiments (see Supporting Information, S8) provide additional evidence of the thermally triggered release of the organic dye from the GNS pattern. The amount of released dye can be estimated from the fluorescence confocal images of the BDP bound to the GNS patterns. To this purpose, we compared the average signal found in Regions of Interest (ROI) on the incubated patterns to those selected on the patterns after heating (15 min, 42 °C). An average value of 30 ± 10% has been obtained by averaging up to 4 ROIs in 3 different fields of view in both conditions. This value is higher than the value obtained from the measurement of the fluorescence signal from the 100 μL supernatant (17 ± 2%) due to the dye stuck into the paper substrate that does not contribute to the releasable fraction.

The release of BDP from the printed GNS surface was also induced by NIR laser irradiation of the patterned paper substrates. As in the previous case, we used printed patterns covered with a thin layer of water (typically: 100 μL on a printed area of 4 mm^2). All measurements were collected 5−6 times on different samples to evaluate the standard error. The percentage of the released BDP-SH (±0.45%) obtained in this way is summarized in Figure 5.

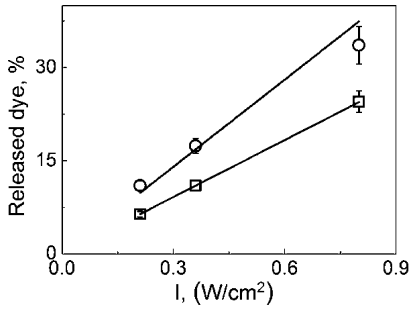

Figure 5. Dependence of NIR-triggered dye release as a function of the irradiation intensity (laser exposure 20 min). The GNS patterns were printed from inks with concentrations C_{GNS} = 0.42 mg/mL, δ = 20402 drops/mm^2 (open squares), and C_{GNS} = 4.2 mg/mL (δ = 20402 drops/mm^2 (open circles)). The solid lines are the best linear fit to the data with slopes: 30 (±1) %/[W/cm^2] and 47 (±3) %/[W/cm^2].

It is clearly seen that in the case of higher concentration of printed GNS higher fractions of released BDP dye can be reached and correspond to approximately 0.15 μg of dye overall released with a release rate of about 0.45 μg/h. It is noteworthy that at I = 0.4 W/cm^2 the fraction of released dye increases by 1.5 times with concentration, while the temperature increases only (see Figure 3) by a factor of 1.2.

A 2-orders of magnitude larger quantity of dye can be grafted (and released) from a monolayer of noble metal nanoparticles.

DOI: 10.1021/acsami.6b02983
ACS Appl. Mater. Interfaces 2016, 8, 9909−9916

However, the maximum amount of dye released by NIR irradiation in our experiments (0.15 μg corresponding to the release rate of ~0.45 μg/h) is still significantly lower than the doses of drugs obtained in commercial transdermal patches. For example, patches loaded with buprenorphine are designed to passively deliver 35, 52.5, or 70 μg h^{-1} of the drug with a maximum dose of 3.36 mg/day.[50]

In our current study local heating and an active release of the model dye are obtained. The amount of released compound seems to be limited mostly by the capability of loading onto the GNS patterns, due to thiol-exchanging process between PEG and BDP dye. Therefore, our studies are now aimed to the attainment of bare printed GNS surface thanks to postprinting treatment. In addition, the GNS density on the patterns can also be improved by changing the printing parameters, e.g., by increasing the printed area and the drop density. Printing polydimethylsiloxane (PDMS) barriers around patterns could also help to avoid the contact of targeted molecules with unprinted substrate, avoiding unnecessary dye adsorption to the paper.

CONCLUSION

In the present work stable GNS-based inks were successfully printed onto pigment-coated paper substrates. The resulted printed patterns showed a significant photothermal effect under NIR irradiation. This photothermal response is much higher with respect to previously studied GNS monolayers on glass surfaces.[21] Indeed, we are able to achieve a temperature ≈45−47 °C (temperatures typically used for hyperthermal treatments in medicine) using low laser intensities ($I \cong 0.2$ W/cm^2) within permitted limits for skin irradiation ($I < 0.3$ W/cm^2).[51] Notably, it is possible to reach pronounced photothermal response of gold patterns printed even with very low GNS concentration (C_{GNS} = 0.042 mg/mL) inks. Moreover, as we show here for a model fluorescent compound, BDP-SH, NIR irradiation at λ = 800 nm triggers the release of substantial fractions (≈30%) of molecules bound to the printed GNS surface. Our future research will be focused on the improvement of drug loading and their active release from patterned gold surfaces by external application of NIR radiation.

ASSOCIATED CONTENT

Supporting Information

The Supporting Information is available free of charge on the ACS Publications website at DOI: 10.1021/acsami.6b02983.

Additional information about experimental and printing details, AFM images of printed patterns, SEM images, additional information about NIR irradiation and dye release from printed surface including fluorescent images (PDF)

Video of drops formation (AVI)

AUTHOR INFORMATION

Corresponding Authors

*E-mail: mykola.borzenkov@unimib.it.

*E-mail: annimaa@gmail.com.

Author Contributions

The manuscript was written through contributions of all authors. All authors have given approval to the final version of the manuscript.

Notes

The authors declare no competing financial interest.

ACKNOWLEDGMENTS

This research was supported by University of Milano-Bicocca within the framework "Bicocca for Expo" fellowships. The author A. Määttänen thankfully acknowledges the Graduate School at Åbo Akademi University for the granted research scholarship for financial support.

REFERENCES

(1) Kamyshny, A.; Steinke, J.; Magdassi, S. Metal-Based Inkjet Inks for Printed Electronics. *Open Appl. Phys. J.* **2011**, *4*, 19−36.

(2) Hudd, A. In *The Chemistry of Inkjet Inks*; Magdassi, S., Ed.; World Scientific: New Jersey-London-Singapore, 2010; pp 3−18.

(3) Singh, M.; Haverinen, H. M.; Dhagat, P.; Jabbour, G. E. Inkjet Printing-Process and its Applications. *Adv. Mater.* **2010**, *22*, 673.

(4) Tekin, E.; Smith, P. J.; Schubert, U. S. Inkjet Printing as a Deposition and Patterning Tool for Polymers and Inorganic Particles. *Soft Matter* **2008**, *4*, 703−713.

(5) Miller, E. D.; Phillippi, J. A.; Fisher, G. W.; Campbell, P. G.; Walker, L. N.; Weiss, L. E. Inkjet Printing of Growth Factor Concentration Gradients and Combinatorial Arrays Immobilized on Biologically-Relevant Substrates. *Comb. Chem. High Throughput Screening* **2009**, *12*, 604−618.

(6) Määttänen, A. K.; Fors, D.; Wang, S.; Valtakari, D.; Ihalainen, P.; Peltonen, J. Paper-Based Planar Reaction Arrays for Printed Diagnostics. *Sens. Actuators, B* **2011**, *160*, 1404−1412.

(7) Cui, X.; Boland, T.; D'Lima, D. D.; Lotz, M. K. Thermal Inkjet Printing in Tissue Engineering and Regenerative Medicine. *Recent Pat. Drug Delivery Formulation* **2012**, *6*, 149−155.

(8) Krause, C. E.; Otieno, B. A.; Latus, A.; Faria, R. C.; Patel, V.; Gutkind, J. S.; Rusling, J. F. Rapid Microfluidic Immunoassays of Cancer Biomarker Proteins Using Disposable Inkjet-Printed Gold Nanoparticles Arrays. *ChemistryOpen* **2013**, *2*, 141−145.

(9) Ihalainen, P.; Pettersson, F.; Pesonen, M.; Viitala, T.; Määttänen, A.; Österbacka, R.; Peltonen, J. An Impedimetric Study of DNA Hybridization on Paper-Supported Inkjet-Printed Gold Electrodes. *Nanotechnology* **2014**, *25*, 094009.

(10) Doraiswamy, A.; Dunaway, T. M.; Wilker, J. J.; Narayan, R. J. Inkjet Printing for Bioadhesives. *J. Biomed. Mater. Res., Part B* **2009**, *89*, 28−35.

(11) Jalo, J.; Sillanpaa, H.; Makinen, R. M. Radio Interface Design for Inkjet-Printed Biosensor Applications. *Prog. Electromagn. Res.* **2013**, *142*, 409−422.

(12) Magdassi, S. In *The Chemistry of Inkjet Inks*; Magdassi, S., Ed.; World Scientific: New Jersey-London-Singapore, 2010; pp 19−41.

(13) Gamerith, S.; Klug, A.; Scheiber, H.; Scherf, U.; Moderegger, E.; List, E. J. Direct Ink-Jet Printing of Ag-Au Nanoparticle and Ag-Precursor Based Electrodes for OFET Application. *Adv. Funct. Mater.* **2007**, *17*, 3111−3118.

(14) Sperling, R. A.; Pilar, R.; Zhang, F.; Zanella, M.; Parak, W. J. Biological Applications of Gold Nanoparticles. *Chem. Soc. Rev.* **2008**, *37*, 1896−1908.

(15) Huang, X. H.; Jain, P. K.; El-Sayed, I. H.; El-Sayed, M. A. Plasmonic Photothermal Therapy (PPTT) Using Gold Nanoparticles. *Lasers Med. Sci.* **2008**, *23*, 217−228.

(16) Dykman, L. A.; Khlebstov, N. G. Gold Nanoparticles in Biology and Medicine: Recent Advances and Prospects. *Acta Naturae.* **2011**, *3*, 34−55.

(17) Yamaguchi, M.; Araga, S.; Mita, M.; Yamasaki, K.; Maekawa, K. On-Demand Infrared Laser Sintering of Gold Nanoparticle Paste for Electrical Contacts. *IEEE Trans. Compon., Packag., Manuf. Technol.* **2015**, *5*, 1160−1168.

(18) Freddi, S.; Sironi, L.; D'Antuono, R.; Morone, D.; Donà, A.; Cabrini, E.; D'Alfonso, L.; Collini, M.; Pallavicini, P.; Baldi, G.; Maggioni, D.; Chirico, G. A Molecular Thermometer for Nanoparticles for Optical Hyperthermia. *Nano Lett.* **2013**, *13*, 2004−2010.

(19) Rodriguez-Oliveros, R.; Sanchez-Gil, J. A. Gold Nanostars as Thermoplasmonic Nanoparticles for Optical Heating. *Opt. Express* **2012**, *20*, 621−626.

(20) Hainfeld, J. F.; Lynn, L.; Slatkin, D. N.; Dilmanian, A. F.; Vadas, T. M.; Smilowitz, H. M. Gold Nanoparticle Hyperthermia Reduces Radiotherapy Doses. *Nanomedicine* **2014**, *10*, 1609−1617.
(21) Pallavicini, P.; Donà, A.; Taglietti, A.; Minzioni, O.; Patrini, M.; Dacarro, G.; Chirico, G.; Sironi, L.; Bloise, N.; Visai, L.; Scarabelli, L. Self-Assembled Monolayers of Gold Nanostars: A Convenient Tool for Near-IR Photothermal Biofilm Eradication. *Chem. Commun.* **2014**, *50*, 1969−1971.
(22) Chen, H.; Zhang, X.; Dai, S.; Ma, Y.; Cui, S.; Achilefus, S.; Gu, Y. Multifunctional Gold Nanostar Conjugates for Tumor Imaging and Combined Photothermal and Chemo-Therapy. *Theranostics* **2013**, *3*, 633−649.
(23) Jensen, G. C.; Krause, C. E.; Sotzing, G. A.; Rusling, J. E. Inkjet-Printed Gold Nanoparticle Electrochemical Arrays on Plastic. Application to Immunodetection of a Cancer Biomarker Protein. *Phys. Chem. Chem. Phys.* **2011**, *13*, 4888−4894.
(24) Määttänen, A.; Vanamo, U.; Ihalainen, P.; Pulkkinen, P.; Tenhu, H.; Bodacka, J.; Peltonen, J. A Low-Cost Paper-Based Inkjet-Printed Platform for Electrochemical Analyses. *Sens. Actuators, B* **2013**, *177*, 153−162.
(25) Marsico, A. L.; Creran, B.; Duncan, B.; Elci, S. G.; Jiang, Y.; Onasch, T. B.; Wormhoudt, J.; Rotello, V. M.; Vachet, R. W. Inkjet-Printed Gold Nanoparticle Surface for the Detection of Low Molecular Weight Biomolecules by Laser Desorption/Ionization Mass Spectrometry. *J. Am. Soc. Mass Spectrom.* **2015**, *26*, 1931−1937.
(26) Benson, J.; Fung, C. M.; Lloyd, J. S.; Deganello, D.; Smith, N. A.; Teng, K. S. Direct Patterning of Gold Nanoparticles Using Flexographic Printing for Biosensing Applications. *Nanoscale Res. Lett.* **2015**, *10*, 127−128.
(27) Tao, H.; Marelli, B.; Yang, M.; An, B.; Onses, M. S.; Rogers, J. A.; Kaplan, D. L.; Omenetto, F. G. Inkjet Printing of Regenerated Silk Fibroin: From Printable Forms to Printable Functions. *Adv. Mater.* **2015**, *27*, 4273−4279.
(28) Hoppmann, E. P.; Wei, W. Yu; White, I. M. Highly Sensitive and Flexible Inkjet Printed SERS Sensors on Paper. *Methods* **2013**, *63*, 219−224.
(29) Casu, A.; Cabrini, E.; Donà, A.; Falqui, A.; Diaz-Fernandez, Y.; Milanese, C.; Taglietti, A.; Pallavicini, P. Controlled Synthesis of Gold Nanostars Using a Zwitterionic Surfactant. *Chem. - Eur. J.* **2012**, *18*, 9381−9390.
(30) Guerrero-Martínez, A.; Barbosa, S.; Pastoriza-Santos, I.; Liz-Marzán, L. M. Nanostars Shine Bright for You. Colloidal Synthrsis, Properties, and Applications. *Curr. Opin. Colloid Interface Sci.* **2011**, *16*, 118−127.
(31) Rodriguez-Oliveros, R.; Sanchez-Gil, J. A. Gold Nanostars as Thermoplasmonic Nanoparticles for Optical Heating. *Opt. Express* **2012**, *20*, 621−626.
(32) Pallavicini, P.; Basile, S.; Chirico, G.; Dacarro, G.; D'Alfonso, L.; Donà, A.; Patrini, M.; Falqui, A.; Sironi, L.; Taglietti, A. Monolayers of Gold Nanostars With Two Near-IR LSPR Capable of Additive Photothermal Response. *Chem. Commun.* **2015**, *51*, 12928−12930.
(33) Sperling, R. A.; Parak, W. J. Surface Modification, Functionalization and Bioconjugation of Colloidal Inorganic Nanoparticles. *Philos. Trans. R. Soc., A* **2010**, *368*, 1333−1383.
(34) Chirico, G.; Pallavicini, P.; Collini, M. Gold Nanostars for Superficial Deseases: a Promising Tool for Localized Hyperthermia? *Nanomedicine* **2014**, *9*, 1−3.
(35) Pallavicini, P.; Chirico, G.; Collini, M.; Dacarro, G.; Doná, A.; D'Alfonso, L.; Falqui, A.; Diaz-Fernandez, Y.; Freddi, S.; Garofalo, B.; Genovese, A.; Sironi, L.; Taglietti, A. Synthesis of Branched Au Nanoparticles With Tunable Near-Infrared LSPR Using a Zwitterionic Surfactant. *Chem. Commun.* **2011**, *47*, 1315−1317.
(36) Hoppmann, E. P.; Wei, W. Yu; White, Ian M. Inkjet-Printed Fluidic Paper Devices for Chemical and Biological Analytics Using Surface Enhanced Raman Spectroscopy. *J. Sel. Top. Quantum Electron.* **2014**, *20*, 7300510.
(37) Yu, W. W.; White, I. M. Inkjet-Printed Paper-Based SERS Dipsticks and Swabs for Trace Chemical Detection. *Analyst* **2013**, *138*, 1020−1025.
(38) Pallavicini, P.; Bernhard, C.; Dacarro, G.; Denat, F.; Diaz-Fernandez, Y.; Goze, C.; Pasotti, L.; Taglietti, A. Optical Method for Predicting the Composition of Self-Assembled Monolayers of Mixed Thiols on Surfaces Coated with Silver Nanoparticles. *Langmuir* **2012**, *28*, 3558−3568.
(39) Sarfraz, J.; Määttänen, A.; Ihalainen, P.; Keppeler, M.; Linden, M.; Peltonen, J. Printed Copper Acetate Based H2S Sensor on Paper Substrate. *Sens. Actuators, B* **2012**, *173*, 868−873.
(40) Määttänen, A.; Fallarero, A.; Kujala, J.; Ihalainen, P.; Vuorela, P.; Peltonen, J. Printed Paper-Based Arrays as Substrates for Biofilm Formation. *AMB Express* **2014**, *4*, 32−44.
(41) Bollström, R.; Määttänen, A.; Tobjörk, D.; Ihalainen, P.; Kaihovirta, N.; Österbacka, R.; Peltonen, J.; Toivakka, M. A Multilayer Coated Fiber-Based Substrate Suitable for Printed Functionality. *Org. Electron.* **2010**, *10*, 1020−1023.
(42) Määttänen, A.; Ihalainen, P.; Bollström, R.; Toivakka, M.; Peltonen, J. Wetting and Print Quality Study of an Inkjet-Printed Poly(3-hexylthiophene) on Pigment Coated Papers. *Colloids Surf., A* **2010**, *367*, 76−84.
(43) Rahme, K.; Chen, L.; Hobbs, R. G.; Morris, M. A.; O'Driscoll, C.; Holmes, J. D. PEGylated Gold Nanoparticles: Polymer Quantification as a Function of PEG Lengths and Nanoparticles Dimensions. *RSC Adv.* **2013**, *3*, 6085−6094.
(44) Manson, J.; Kumar, D.; Meenan, B. J.; Dixon, D. Polyethylene Glycol Functionalized Gold Nanoparticles: The Influence of Capping Density in Various Media. *Gold Bull.* **2011**, *44*, 99−105.
(45) Zhu, J.; Chin, J.; Wängler, B.; Lennox, R. B.; Schirrmacher, R. Rapid (18)F-Labeling and Loading of PEGylated Gold Nanoparticles for In Vivo Applications. *Bioconjugate Chem.* **2014**, *25*, 1143−1150.
(46) Borzenkov, M.; Chirico, G.; D'Alfonso, L.; Sironi, L.; Collini, M.; Cabrini, E.; Dacarro, G.; Milanese, C.; Pallavicini, P.; Taglietti, A.; Bernhard, C.; Denat, F. Thermal and Chemical Stability of Thiol Bonding on Gold Nanostars. *Langmuir* **2015**, *31*, 8081−8091.
(47) Jain, P. K.; Lee, K.-S.; El-Sayed, I. H.; El-Sayed, M. A. Calculated Absorption and Scattering Properties of Gold Nanoparticles of Different Size, Shape, and Composition: Applications in Biological Imaging and Biomedicine. *J. Phys. Chem. B* **2006**, *110*, 7238−7248.
(48) Stephan, K.; Laesecke, A. The Thermal Conductivity of Fluid Air. *J. Phys. Chem. Ref. Data* **1985**, *14*, 227−234.
(49) Rurack, K.; Martinez, R. *The Supramolecular Chemistry of Organic-Inorganic Hybrid Materials*; John Willey & Sons, Inc: Hoboken, 2010.
(50) Margetts, L.; Sawyer, L. Transdermal Drug Delivery: Principles and Opioid Therapy. *Med. Health* **2007**, *7*, 171−176.
(51) International Commission on Non-Ionizing Radiation Protection. ICNIRP Guidelines on Limits of Exposure to Laser Radiation of Wavelengths between 180 nm and 1,000 μm. *Health Phys.* **2013**, *105*, 271−295.

DOI: 10.1021/acsami.6b02983
ACS Appl. Mater. Interfaces 2016, 8, 9909−9916